Supporting Information

Imidazolium-Tethered Red-Emissive Iridium AIEgen for Sensitive Detection of NAD(P)H in Aqueous and Cellular Media

Aryan Gautam,[1] Ajay Gupta,[1] Deepika Chauhan,[1] Amit Kunwar,[2,3,*] and Pijus K. Sasmal[1,4,*]

[1]School of Physical Sciences, Jawaharlal Nehru University, New Delhi 110067, India.

[2]Radiation and Photochemistry Division, Bhabha Atomic Research Centre, Anushaktinagar, Mumbai 400085, India.

[3]Homi Bhabha National Institute, Anushaktinagar, Mumbai – 400094, India.

[4]School of Chemistry, University of Hyderabad, Hyderabad 500046, India.

**Corresponding authors: kamit@barc.gov.in (A. Kunwar) and pijus@mail.jnu.ac.in; pijussasmal@uohyd.ac.in; pijussasmal@gmail.com (P. K. Sasmal)*

Table of Contents

Supplementary Scheme

Scheme S1. Chemical structures of the probes **Ir1-Ir3**.

Supplementary Tables

Table S1. Limit of detection (LOD) of the probes **Ir1-Ir3** towards NAD(P)H.

Table S2. Comparison of this study with previously reported NAD(P)H probes.

Table S3. Hydrodynamic diameters (d) of probes **Ir1** and **Ir2** in the absence and presence of NAD(P)H.

Table S4. Zeta potential (ζ) of the probe **Ir2** towards NAD(P)H.

Supplementary Figures

Fig. S1-S2 ^{1}H and ^{13}C NMR spectra of compound **1** in $CDCl_3$.

Fig. S3-S4 ^{1}H and ^{13}C NMR spectra of compound **2** in DMSO-d_6.

Fig. S5-S6 ^{1}H and ^{13}C NMR spectra of probe **Ir2** in $CDCl_3$.

Fig. S7 ESI-HRMS spectrum of compound **2**.

Fig. S8 ESI-HRMS spectrum of probe **Ir2**.

Fig. S9 HPLC chromatogram of probe **Ir2**.

Fig. S10 Absorption and emission spectra of probe **Ir2**.

Fig. S11 Emission decay curve of the probe **Ir2**.

Fig. S12 Stability of the probe **Ir2** in PBS.

Fig. S13 Titration spectra of the **Ir2** upon the addition of NADH.

Fig. S14 NADPH detection by **Ir2** in various buffer systems.

Fig. S15 NAD(P)H imaging in presence of different concentration of exogenous glucose.

Fig. S16 NAD(P)H imaging in non-cancer and cancer cells.

Fig. S17 Plot of cell viability by MTT assay of the probe **Ir2** in MCF-7 cells.

Fig. S18 Plot of cell viability by MTT assay of the probe **Ir2** in A549 cells.

Supplementary References

1. Materials

Dichloromethane (CH_2Cl_2) and methanol (MeOH) were distilled under argon from calcium hydride and magnesium chips, respectively. Acetonitrile (MeCN), diethyl ether (Et_2O), and dimethyl sulfoxide (DMSO) were used as dry, HPLC-grade solvents without additional drying. All reactions were carried out under an argon atmosphere. 2-Phenylquinoline (PQ), 2,2′-bipyridine-4,4′-dicarboxylic acid, 1-(3-aminopropyl)imidazole, triethylamine (Et_3N), nicotinamide adenine dinucleotide (NADH) and its phosphorylated counterpart (NADPH) were procured from Sigma-Aldrich. $IrCl_3 \cdot 3H_2O$ and potassium carbonate were purchased from Alfa-Aesar. Thionyl chloride, methyl iodide, and potassium hydroxide were obtained from Central Drug House (CDH). Thin-layer chromatography (TLC) plates were sourced from Merck (Germany). Dulbecco's Modified Eagle Medium (DMEM), Dulbecco's phosphate-buffered saline (PBS), trypsin, penicillin-streptomycin (pen-strep) solution, fetal bovine serum (FBS), and 3-(4,5-dimethylthiazol-2-yl)-2,5-diphenyltetrazolium bromide (MTT) were purchased from Thermo Fisher Scientific. Hoechst 33342 was obtained from Invitrogen. A549, MCF-7, and NIH/3T3 cells were procured from the Cell Repository at the National Centre for Cell Science (NCCS), Pune. Double-distilled water and Milli-Q water (~18.8 mΩ·cm resistivity, CDUFBI001, Millipore, USA) were used in the preparation of all aqueous solutions. The iridium dimer $[Ir(PQ)_2Cl]_2$ was synthesized following a previously reported procedure.[1] Similarly, 4'-(ethoxycarbonyl)-[2,2'-bipyridine]-4-carboxylic acid was prepared as described in the literature.[2] The purity of the synthesized probe **Ir2** was confirmed to be ≥95% based on NMR, high-resolution mass spectrometry (HRMS), and reverse-phase high-performance liquid chromatography (RP-HPLC).

2. Instruments

TLC analysis was carried out on aluminum plates coated with silica gel containing a fluorescent indicator. Compound purification was achieved via column chromatography using silica gel with a particle size of 60–120 mesh. ^1H and ^{13}C NMR spectra were recorded on a Bruker 500 MHz spectrometer at room temperature using $CDCl_3$ and DMSO-d_6 as solvents, with tetramethylsilane (TMS) serving as the internal reference. The NMR chemical shift standards were as follows: for ^1H NMR, $CDCl_3$ at 7.26 ppm and DMSO-d_6 at 2.50 ppm; for ^{13}C NMR, $CDCl_3$ at 77.00 ppm and DMSO-d_6 at 39.52 ppm. All chemical shifts (δ) are reported in parts per million (ppm) relative to TMS. Signal multiplicities were described as singlet (s), doublet (d), triplet (t), doublet of doublets (dd), multiplet (m), and broad (br), with coupling constants (J) expressed in Hertz (Hz). High-resolution electrospray ionization mass spectra (ESI-HRMS) were obtained using a Waters Synapt G2 high-definition mass spectrometer. Fourier transform infrared (FT-IR) spectra were collected on a Shimadzu IR Affinity-1S spectrophotometer (Kyoto, Japan) equipped with a single reflection attenuated total reflectance (ATR) accessory. Spectra were recorded over the range of 4000 to 450 cm^{-1} with a resolution of 4 cm^{-1} and 45 scans per sample. In the IR spectra, peak shapes and intensities were designated as broad (br), very strong (vs), strong (s), medium (m), and weak (w). The purity of the samples was assessed using an

analytical HPLC system (Thermo Scientific Dionex Ultimate 3000) fitted with a UV-Vis detector and a reversed-phase C18 column (Acclaim, 250 mm length, 4.6 mm internal diameter, 5 μm particle size, 120 Å pore size) operated at room temperature. Absorption and emission spectra, along with quantum yields, were measured using a SpectraMax M2 plate reader (Molecular Devices) and an Edinburgh Instruments F900 fluorescence spectrophotometer. Dynamic light scattering (DLS) analyses were performed on a Zetasizer Nano ZS90 (Malvern Instruments, Worcestershire, UK). All luminescence measurements were conducted under aerated conditions.

3. Methods

3.1 Probe purity

The purity of probe **Ir2** was evaluated using reverse-phase high-performance liquid chromatography (RP-HPLC).[3] A 20 μL aliquot of 50 μM of **Ir2** solution in H_2O/acetonitrile (80:20 v/v) was injected into a reversed-phase HPLC column. Detection was carried out at a wavelength of 254 nm. HPLC-grade acetonitrile (MeCN) and Millipore water containing 0.1% trifluoroacetic acid (TFA, v/v) served as the mobile phase. The elution gradient was programmed from 95% water and 5% MeCN to 50% water and 50% MeCN over 30 min, at a constant flow rate of 1 mL min^{-1}.

3.2 UV-visible spectra

The absorption spectra of probe **Ir2** was recorded in water containing 0.2% DMSO at room temperature. All UV-Vis measurements were conducted using quartz cuvettes with a 10 mm path length, and wavelengths are reported in nanometers (nm).

3.3 Emission spectra and determination of quantum yield

The emission spectra of probe **Ir2** were recorded in water containing 1% DMSO at room temperature using a quartz cuvette with a 10 mm optical path length. Excitation was performed at 425 nm. The quantum yield (Φ) was determined in MeCN at room temperature using $[Ru(bpy)_3](PF_6)_2$ (Φ = 0.0504) as the reference standard.

3.4 Stability studies

The stability of probe **Ir2** was evaluated by UV-Vis spectroscopy in PBS (10 mM, pH 7.4).[3] Briefly, the complex (20 μM) was dissolved in PBS containing 0.4% DMSO and monitored at room temperature over various time points for up to 24 h using UV-Vis spectroscopy.

3.5 Determination of lipophilicity

The lipophilicity (log $P_{o/w}$) of the probe was determined using the classical flask-shaking method.[3] Briefly, 0.5 mg of each probe was added to 3 mL of a 1:1 (v/v) mixture of *n*-octanol and water, followed by vigorous mixing for 24 h. The mixture was then left undisturbed for an additional 24 h to allow phase equilibrium. After separation of two layers, the concentration of the probe in the *n*-octanol (C_o) and water (C_w) phases were measured by UV-vis spectroscopy, and the partition coefficient was calculated as log $P_{o/w}$ = log $[C]_o/[C]_w$ value.

3.6 Aggregation-induced emission studies

Aggregation-induced emission (AIE) experiments were carried out by preparing **Ir2** (50 μM) in water containing 1% DMSO, with a final volume of 2 mL. Incremental amounts of THF were added to this solution while maintaining a constant total volume of 2 mL, and the resulting phosphorescence emission spectra were recorded. Dynamic light scattering (DLS) was used to measure the hydrodynamic diameter (d) of **Ir2** in pure aqueous solution as well as in the water–THF mixtures where aggregation occurred.

3.7 Determination of limit of detection (LOD) for NAD(P)H

A 50 μM solution of probe **Ir2** was prepared in water containing 1% DMSO, with a total volume of 2 mL. The probe was titrated with incremental addition of NADH and NADPH at room temperature, and its emission spectra were recorded 2 min after each addition. A plot of emission intensity at the emission maximum *versus* the concentration of NADH or NADPH displayed a linear dynamic response. The limit of detection (LOD) for NAD(P)H was calculated using the following equation:

$$LOD = 3\sigma/S$$

where σ represents the standard deviation from six independent measurements of the emission intensity of the **Ir2** in the absence of NAD(P)H, and S is the slope obtained from the linear regression of the titration curve.

3.8 Characterization of Ir2–NAD(P)H aggregates by DLS

The hydrodynamic diameters (d) of **Ir2** and **Ir2–**NAD(P)H aggregates were measured using dynamic light scattering (DLS). Aqueous solutions containing 50 μM of the probe, with or without 3 μM of NADH or NADPH, were prepared in a total volume of 2 mL with 1% (v/v) DMSO in water. DLS measurements were performed at 25 °C using a 4 mW laser operating at 632.8 nm, with detection at a 90º angle.

3.9 Zeta (ξ) potential measurements

The zeta potential of probe **Ir2** (50 μM), in the presence and absence of 3 μM NADH or NADPH, was measured at 25 ºC in a 1 mL cuvette containing 1% (v/v) DMSO in water. A voltage of 100 V was applied during the measurements.

3.10 Selectivity of Ir2 towards NAD(P)H in the presence of biologically relevant species

The selectivity of probe **Ir2** (50 μM) toward NAD(P)H (6 μM) was evaluated in aqueous solution containing 1% (v/v) DMSO, with a total volume of 200 μL, in the presence of various biologically relevant interfering species at room temperature. Emission intensity measurements were performed using a SpectraMax® M2e fluorescence microplate reader (Molecular Devices LLC, USA) in 96-well plates, with an excitation wavelength of 425 nm, a 660 nm cut-off filter, and emission recorded at 690 nm. Cationic salts—NaCl (Na^+), KCl (K^+), $MgCl_2$ (Mg^{2+}), $CaCl_2$ (Ca^{2+}), $MnCl_2$ (Mn^{2+}), $FeCl_3$ (Fe^{3+}), $CuCl_2$ (Cu^{2+}), and $ZnCl_2$ (Zn^{2+})—were tested at concentrations of 100 μM. Competing biomolecules, including ammonium chloride (NH_4Cl), sodium acetate (NaOAc), sodium dihydrogen

phosphate (NaH_2PO_4), aspartic acid (Asp), glutamic acid (Glu), glycine (Gly), cysteine (Cys), methionine (Met), tyrosine (Tyr), lysine (Lys), urea, glutathione (GSH), glucose, adenosine diphosphate (ADP), adenosine triphosphate (ATP), NADH, and NADPH, were used at 10 μM. Calf thymus DNA (ct-DNA) was included at a concentration of 2 mg/L.

3.11 Colocalization studies

The intracellular localization of **Ir2** was investigated using confocal microscopy. For this, A549 cells were seeded on coverslips at a density of 10^5 cells per well 24 h prior to the experiment. The cells were then treated with the probe **Ir2** (10 μM) for 1 h in DMEM complete media. Following treatment, the cells were washed with 1X PBS and simultaneously stained with MitoTracker Green FM (150 nM) and Hoechst (1 μM) for 30 min. The media were then removed, and the cells were thoroughly washed with PBS (4 x 1 mL) before microscopy imaging. The stained cells were visualized under a Nikon Eclipse Ti-E microscope. Hoechst and **Ir2** were both excited with a 405 nm laser. Hoechst emission was recorded in channel 1 with a bandpass filter range of 450/50 nm, while **Ir2** emission was recorded in channel 3 with a long pass filter range of 595/50 nm. MitoTracker Green emission was captured in channel 2 using a bandpass filter range of 540/30 nm. The obtained images were analysed using Fiji software (NIH), and the extent of co-localization was determined using scatter plot with Pearson's correlation coefficient (PCC).

3.12 Imaging of NAD(P)H in live cells

All experiments were performed in live cells to avoid artifacts associated with fixation procedures.

NAD(P)H imaging: Three sets of experiments were conducted using A549 cells. For this, cells were seeded on coverslips at a density of 10^5 cells per well 24 h prior to the experiments. In the first set, cells were treated with **Ir2** (10 μM) for 30 min. In the second and third sets, cells were incubated with 20 and 50 μM NADH, for 30 min, respectively, followed by treatment with **Ir2** (10 μM) and incubated for an additional 30 min before imaging.

Change in NAD(P)H levels in presence of glucose: This experiment was conducted using the same procedure described for NAD(P)H imaging above, except that 10 and 20 mM glucose were used in place of 20 and 50 μM NADH, respectively.

Fluctuations of NAD(P)H levels in presence of rotenone and FCCP: Seven sets of experiments were carried out using A549 cells. Cells were seeded on coverslips at a density of 10^5 cells per well and allowed to adhere for 24 h prior to treatment. In the first set, cells were treated with **Ir2** (10 μM) for 30 min. In the second, third, and fourth sets, cells were pre-incubated with rotenone at concentrations of 5, 10, and 20 μM, respectively, for 30 min, followed by treatment with **Ir2** (10 μM) for an additional 30 min. In the fifth, sixth, and seventh sets, cells were pre-incubated with FCCP at 5, 10, and 20 μM, respectively, for 30 min, followed by **Ir2** (10 μM) treatment for 30 min. After each treatment, the cells were imaged using a Nikon Eclipse Ti-E fluorescence microscope.

3.13 Cell viability assay

The cytotoxicity of probe **Ir2** was evaluated in A549 and MCF-7 cells using the MTT assay. Stock solutions of **Ir2** were prepared in DMSO. Cultured cells were seeded in 96-well plates in penta-triplicate at a density of 9,000 cells per well. After 24 h of incubation, the culture medium was removed and replaced with fresh medium containing the probe at eight increasing concentrations, ensuring the final DMSO content remained below 1% (v/v). The total volume in each well was maintained at 200 µL. Cells were then incubated with the probe for 24 h, after which the medium was replaced with 200 µL of incomplete medium containing MTT (0.5 mg mL^{-1} in PBS), followed by a 4 h incubation at 37 °C. The medium was then removed and replaced with 200 µL of DMSO to solubilize the formazan crystals, and the plates were incubated at room temperature for 15 min. Absorbance was measured at 570 nm using a SpectraMax spectrophotometer (Molecular Devices), and the resulting data were analyzed using Origin 18 software.

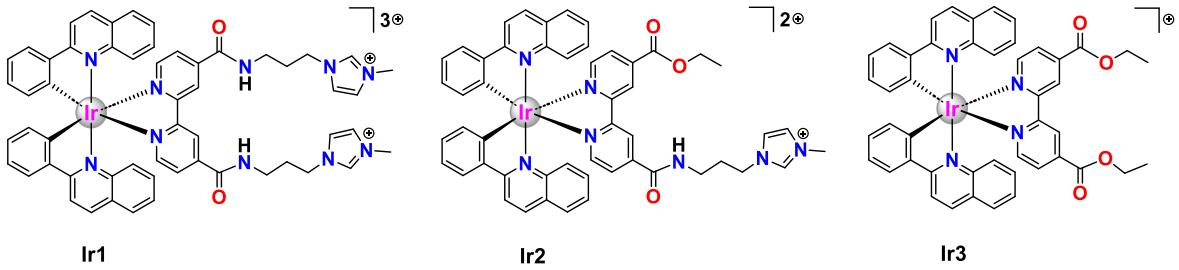

Scheme S1. Chemical structures of the probes **Ir1-Ir3**.

Table S1. The limit of detection (LOD) values of the probes **Ir1-Ir3** for NAD(P)H.

Probes	NADH	NADPH
Ir1	20 ± 0.9 nM	22.1 ± 1.1 nM
Ir2	6.2 ± 0.5 nM	3.6 ± 0.8 nM
Ir3	760 nM	540 nM

Table S2. Comparison of this study with previously reported NAD(P)H probes.

Probe	Detection medium	$\lambda_{ex}/\lambda_{em}$ (nm)	Detection time	LOD	NIR emission	In cell	Organelle localization	Ref.
RA-Resa	10 mM PBS buffer, pH 7.4	480/575	25 min	84 nM	No	Yes	Cytoplasm	4
Indicator 1	25 mM PIPES, 101 mM NaCl, pH 7.0	537/561	5 min	0.1 μM	No	Yes	Cytoplasm	5
MQR	10 mM PBS buffer, pH 7.4	525/548	2 h	Not reported	No	Yes	Cytosol	6
TCF-MQ	10 mM PBS buffer, pH 7.4	582/610	25 min	6 nM	No	Yes	Not reported	7
MQN	PBS buffer, pH 7.4	390/460 450/550	50 min	1.07 μM 1.11 μM	No	Yes	Mitochondria and lysosomes	8
NADH-R	10 mM PBS buffer, pH 7.4	610/657	25 min	12 nM	Yes	Yes	Shifts from Mitochondria to Nucleus	9
QB	20 mM PBS buffer, pH 7.4	630/686	6 min	43 nM	Yes	Yes	Mitochondria	10
ISQM	10 mM PBS buffer, pH 7.4	450/560	< 1 min	59 nM	No	Yes	Mitochondria	11
A, B	PBS buffer, pH 7.4	533/572 535/586	6 min	0.08 μM 0.54 μM	No	Yes	Mitochondria	12
IM-PDAs	10 mM HEPES buffer, pH 7.4	495/549	Not reported	23.5 nM	No	No	No	13
Probe 1	25 mM PIPES buffer, pH 7.4	570/615	23 h	1.2 μM	No	Yes	Mitochondria	14
Complex 1	DI water, pH 7.0	460/539	<30 min	Not reported	No	Yes	Cytoplasm	15
FMA	Buffer solution, pH 7.2	—/524	30 min	1.2 μM	No	No	No	16
UQ-Rh	PBS buffer, pH 7.4	488/520	10 min	Not reported	No	Yes	Cytosol	17
C4D	10 mM HEPES buffer, pH 7.4	275/325	Not reported	24.5 nM	No	No	No	18
DCI-MQ	10 mM PBS buffer, pH 7.4	568/660	15 min	12 nM	Yes	Yes	Mitochondria	19
NAFP4	10 mM PBS buffer	553/584	3 min	3.66 nM	No	Yes	Mitochondria	20

3Q-2	DMSO/PBS buffer (1:1, v/v)	595/670	20 min	Not reported	Yes	Yes	Cytoplasm and Mitochondria	21
DPMQL1	EtOH/PBS buffer (10 mM, pH 7.4, 1:1 v/v)	510/624	60 min	0.36 nM	No	Yes	Mitochondria	22
Cy-N	0.1 M PBS buffer, pH 7.4	720/783	20 min	1.67 μM	Yes	Yes	Not reported	23
Probe 1	10 mM PBS buffer, pH 7.4	590/640	80 min	0.1 μM	No	Yes	Not reported	24
P_{NADH}	PBS buffer, pH 7.4	510/552	40 min	1.25 μM	No	Yes	Cytoplasm	25
LV-2	EtOH/0.1 mM PBS buffer, pH 7.4, 1:9 v/v)	560/650	10 min	Not reported	Yes	Yes	Not reported	26
MC_{2P}	PBS buffer, pH 7.4	390/460	40 min	0.52 μM	No	Yes	Mitochondria	27
Mito-FCC	20 mM PBS buffer, pH 7.4	475/580	10 min	0.26 μM	No	Yes	Mitochondria	28
A1TB	20 mM Tris-HCl buffer, pH 7.4	340/545	5 min	Not reported	No	No	No	29
QAIC	HEPES buffer, pH 7.4	475/555	2 h	25.6 nM	No	Yes	Mitochondria	30
Ir1	DI water, pH 7.0	425/692	2 min	22 nM	Yes	Yes	Mitochondria	3
Ir2	DI water, pH 7.0	425/663	2 min	3.6 nM	Yes	Yes	Mitochondria	***This study***

Table S3. Comparison of hydrodynamic diameters of the probes **Ir1** and **Ir2** in the absence and presence of NAD(P)H.

Probes	hydrodynamic diameter (d)/nm		
	Probe only	NADH	NADPH
Ir1	139	190	225
Ir2	142	220	255

Table S4. Measurement of zeta potential (ζ) (mV) of probe **Ir2** with varying concentrations of NAD(P)H.

$\zeta_{[\mathbf{Ir2}.\mathrm{NAD(P)H}]}$	Concentration of NAD(P)H (μM)			
	0	1	2	3
$\zeta_{[\mathbf{Ir2}.\mathrm{NADH}]}$	51.4	32.1	29.5	30.8
$\zeta_{[\mathbf{Ir2}.\mathrm{NADPH}]}$	51.4	7.3	0.2	-2.9

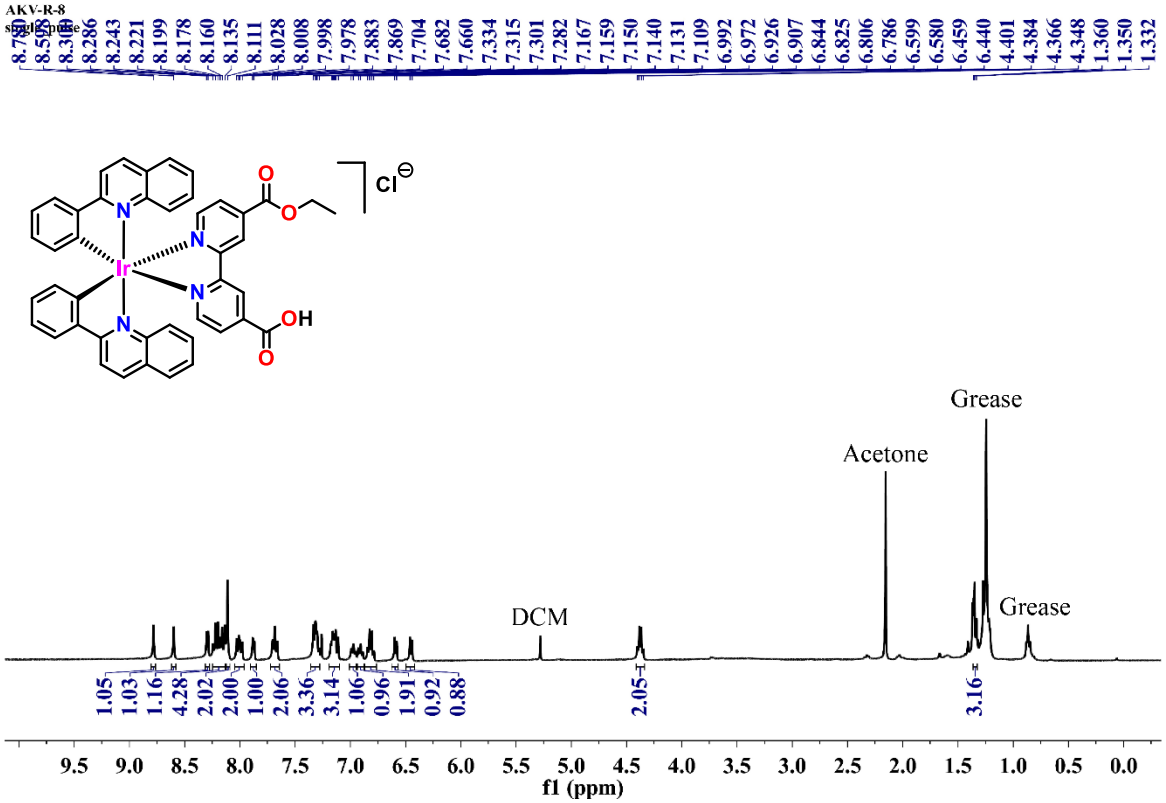

Fig. S1 ^{1}H-NMR spectrum of compound **1** in $CDCl_3$ at 298K.

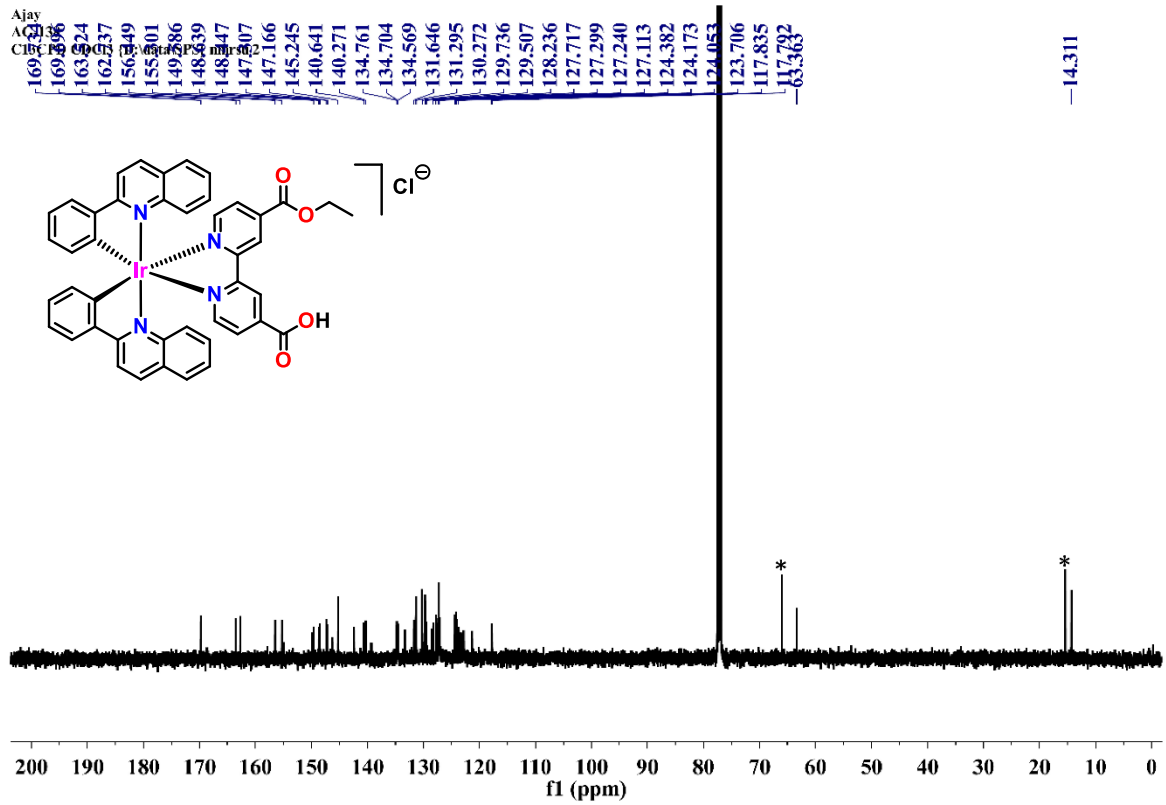

Fig. S2 ^{13}C-NMR spectrum of compound **1** in $CDCl_3$ at 298K. *Et_2O.

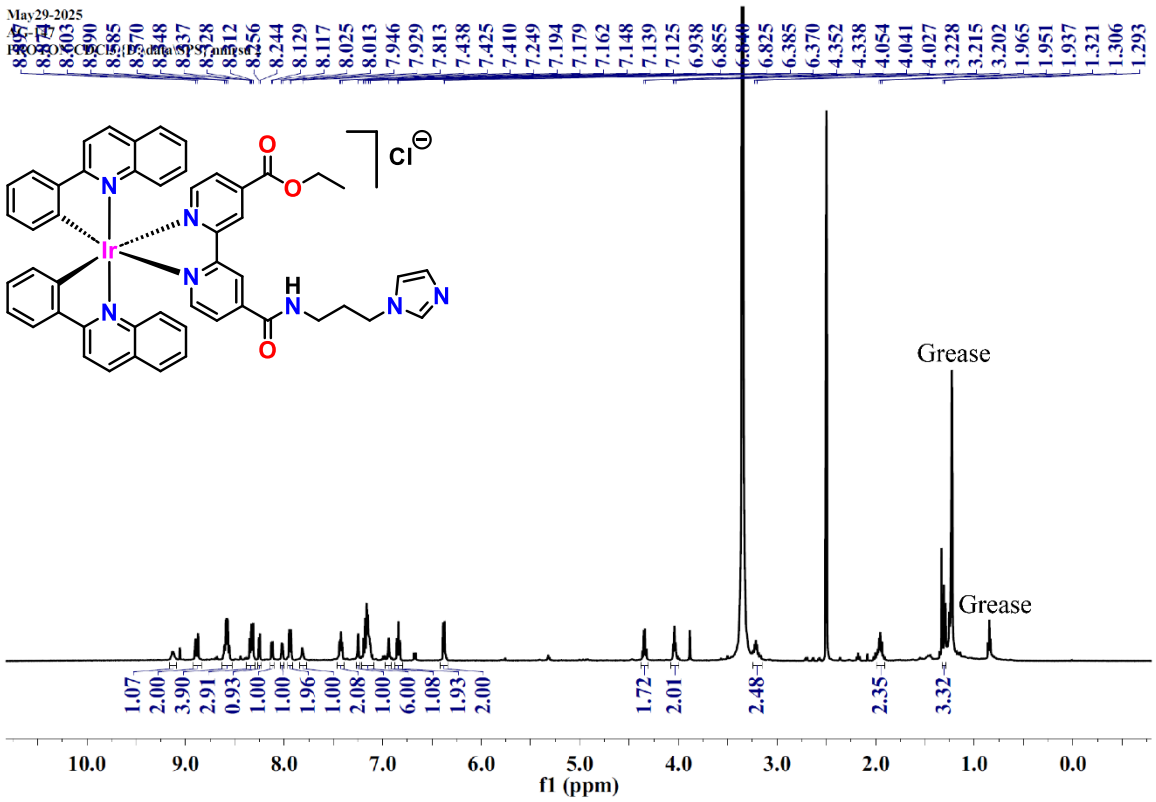

Fig. S3 ^{1}H-NMR spectrum of compound **2** in DMSO-d_6 at 298K.

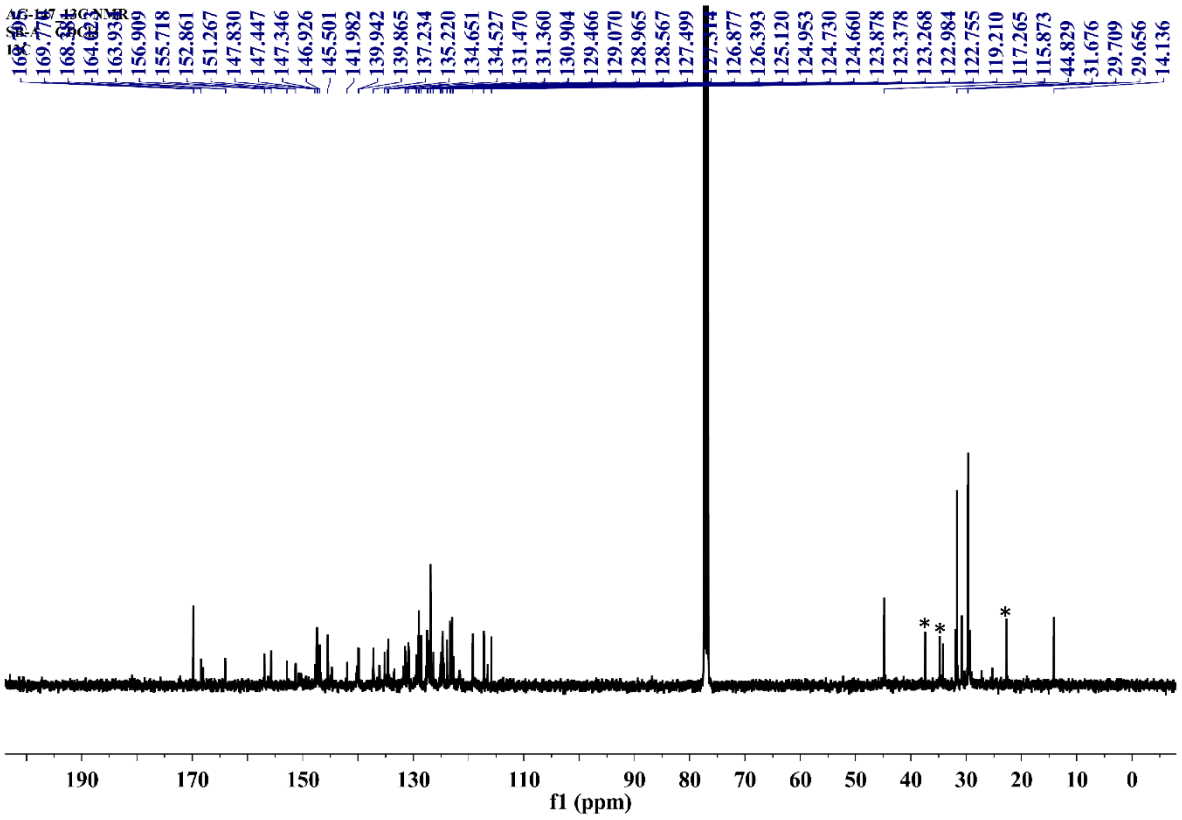

Fig. S4 ^{13}C-NMR spectrum of probe **Ir2** in $CDCl_3$ at 298K. *Grease, n-pentane.

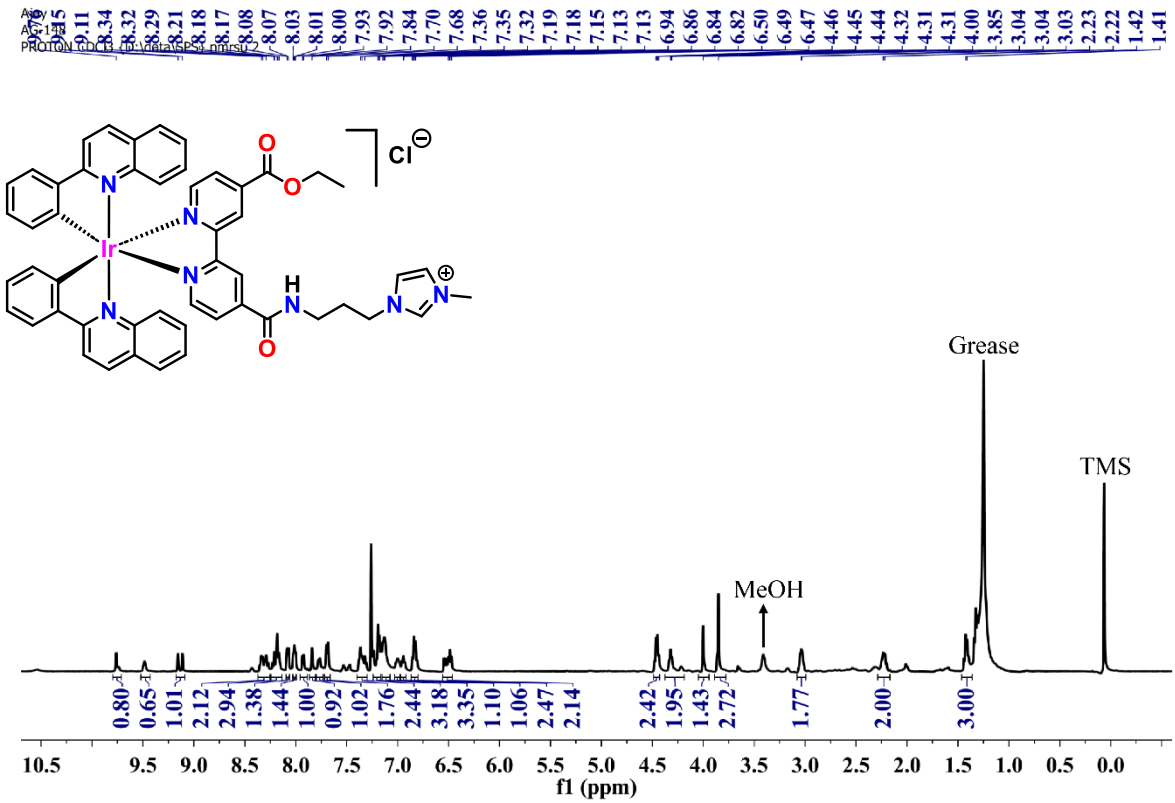

Fig. S5 ^{1}H-NMR spectrum of probe **Ir2** in $CDCl_3$ at 298K.

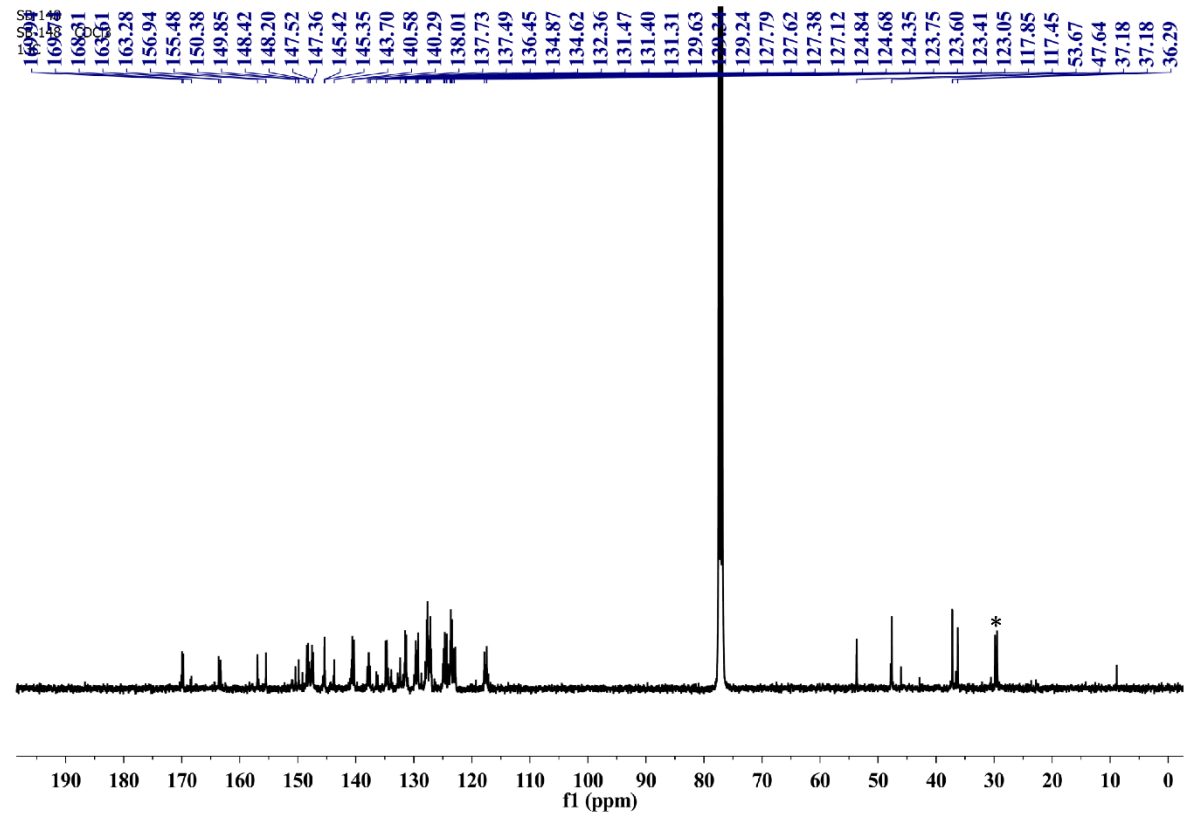

Fig. S6 ^{13}C-NMR spectrum of probe **Ir2** in $CDCl_3$ at 298K. *Grease.

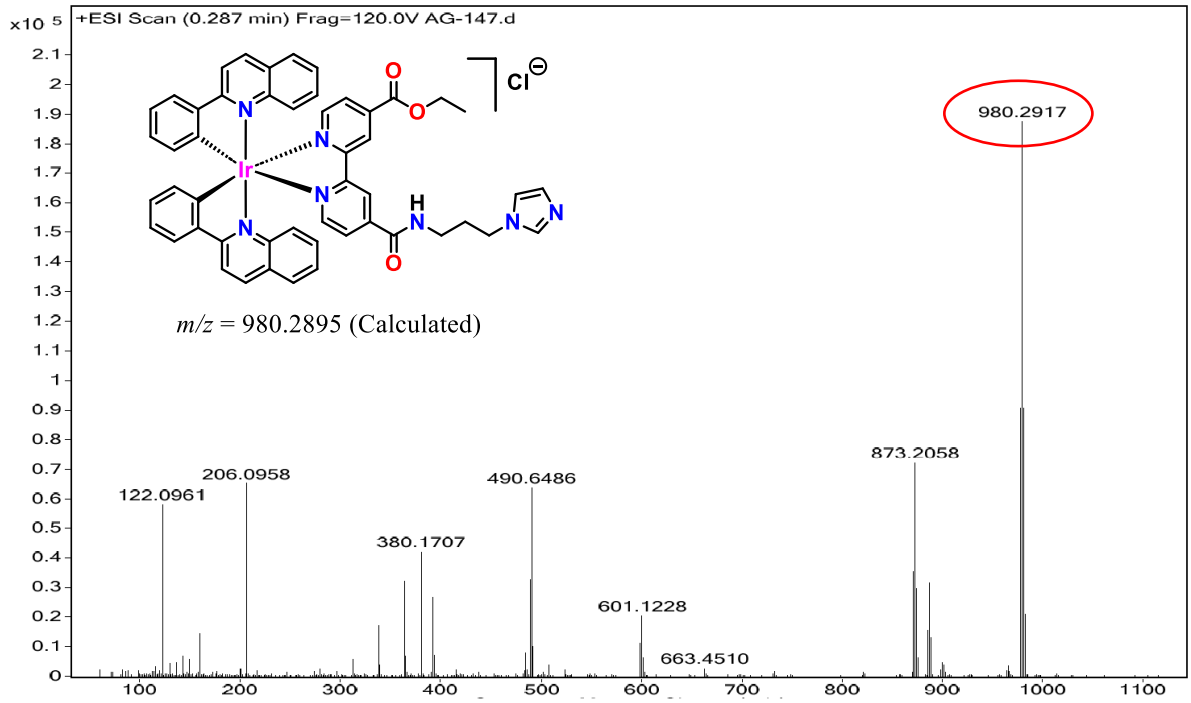

Fig. S7 Mass spectrum of compound **2** in DCM/MeOH at 298K. The peak at *m/z* 980.2917 assignable to $[M]^{+}$.

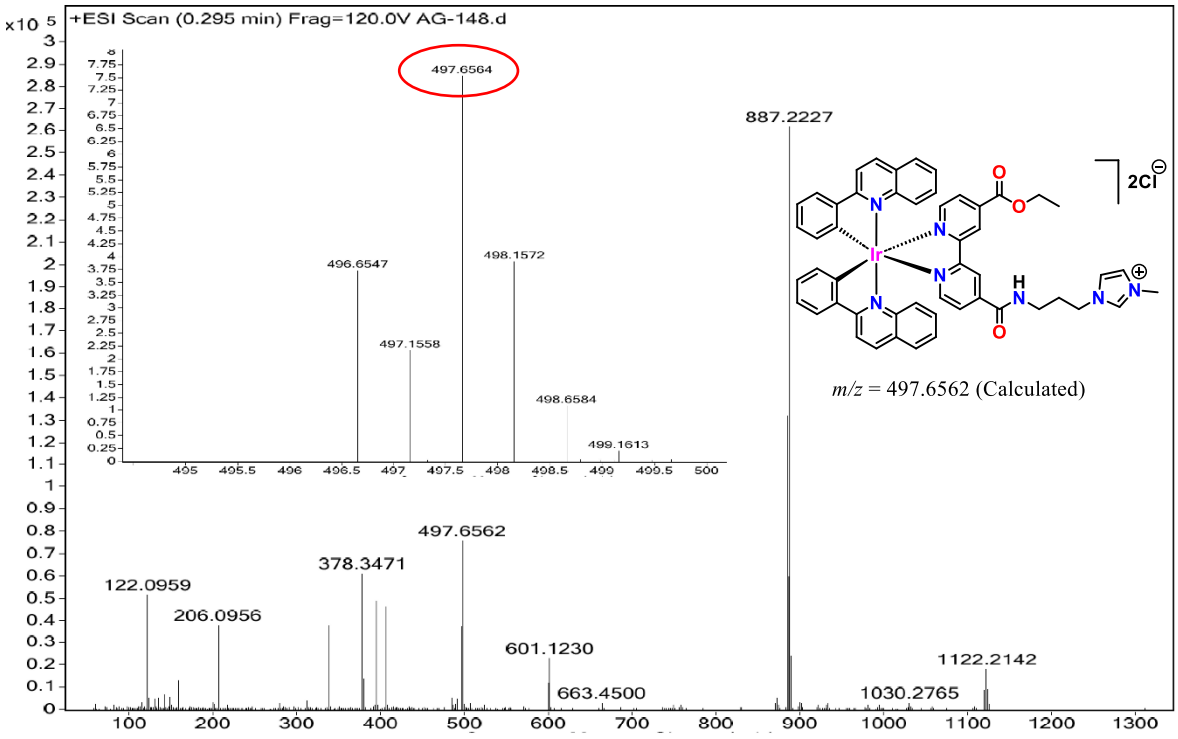

Fig. S8 Mass spectrum of **Ir2** in DCM/MeOH at 298K. The peak at *m/z* 497.6564 is assignable to $[M]^{2+}$, while the peak at *m/z* 887.2227 corresponds to the formation of a methoxy ester species resulting from fragmentation of the amide linkage.

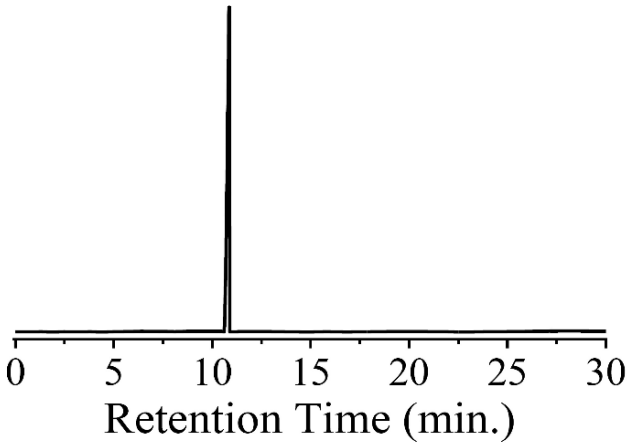

Fig. S9 HPLC chromatogram of **Ir2**, confirming the purity of the probe.

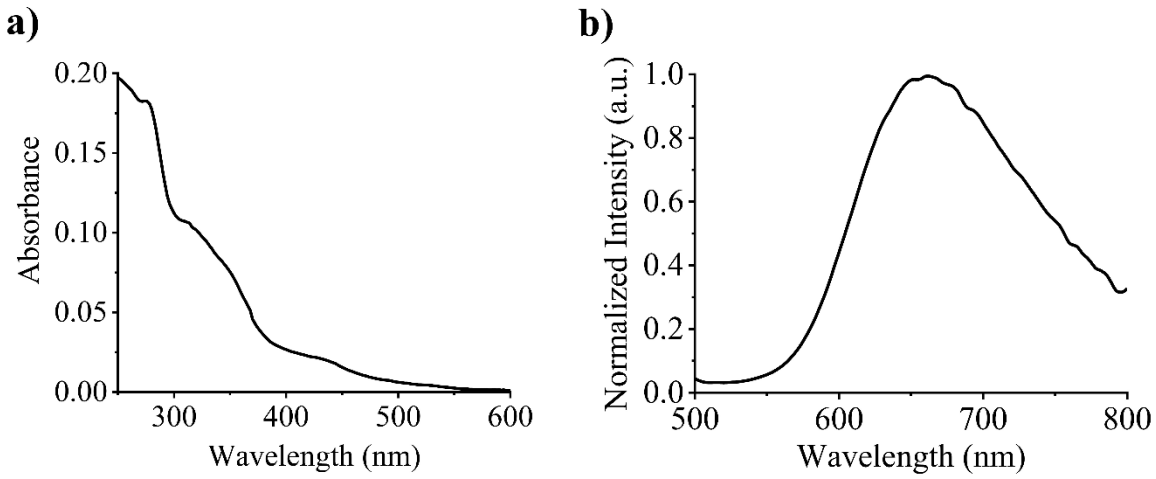

Fig. S10 (a) Absorption spectrum of **Ir2** (10 μM) and (b) normalized emission spectrum of **Ir2** (50 μM), recorded in water at room temperature containing 0.2% and 1% DMSO, respectively. Emission spectra were obtained upon excitation at 425 nm.

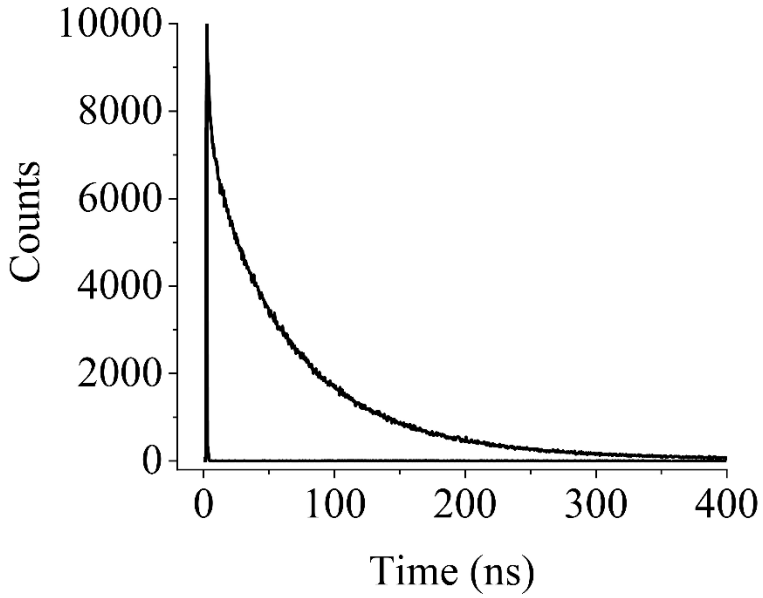

Fig. S11 Emission decay curve of probe **Ir2** recorded in air-saturated MeCN at room temperature.

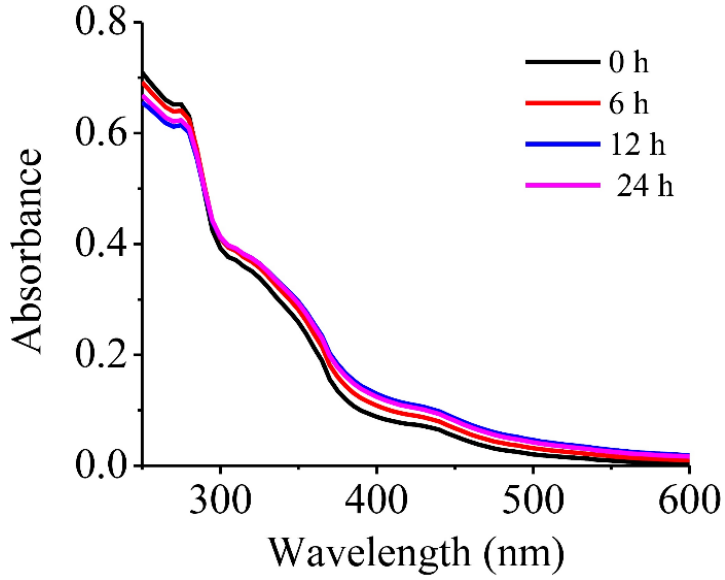

Fig. S12 Stability profile of probe **Ir2** in PBS (10 mM, pH 7.4) at room temperature over a period of 24 h.

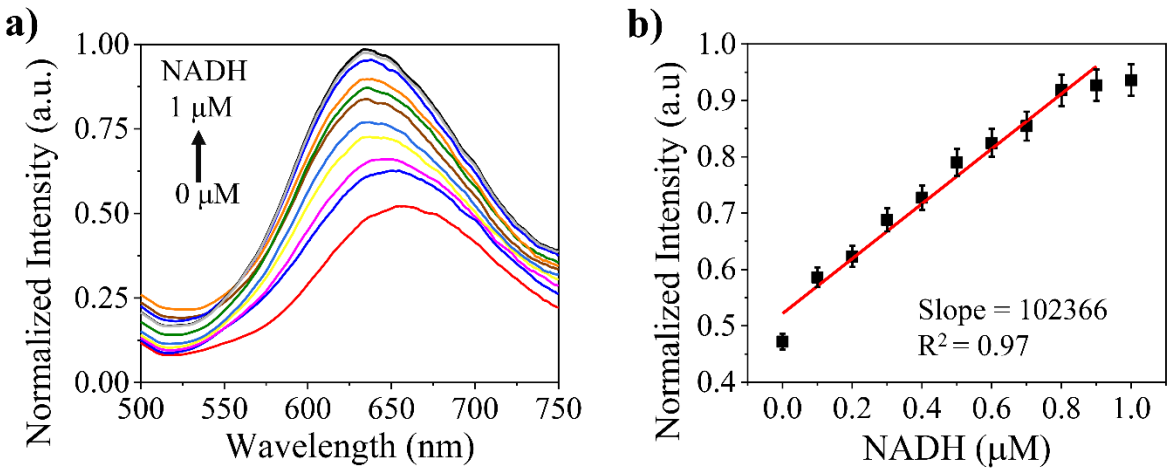

Fig. S13 (a) Phosphorescence titration spectra of probe **Ir2** (50 μM) in aqueous medium with increasing concentrations of NADH (0–1 μM). (B) Linear-fit plot of phosphorescence intensity at 663 nm *versus* NADH concentration in the range of 0–0.9 μM.

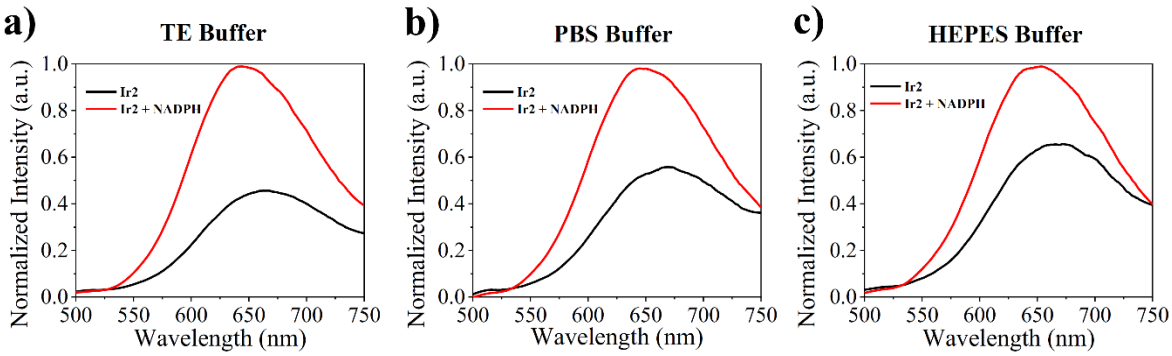

Fig. S14 Phosphorescence emission spectra of **Ir2** (50 μM) in the absence and presence of NADPH (6 μM) in (a) 10 mM TE buffer, (b) 10 mM PBS buffer, and (c) 10 mM HEPES buffer at pH 8.3.

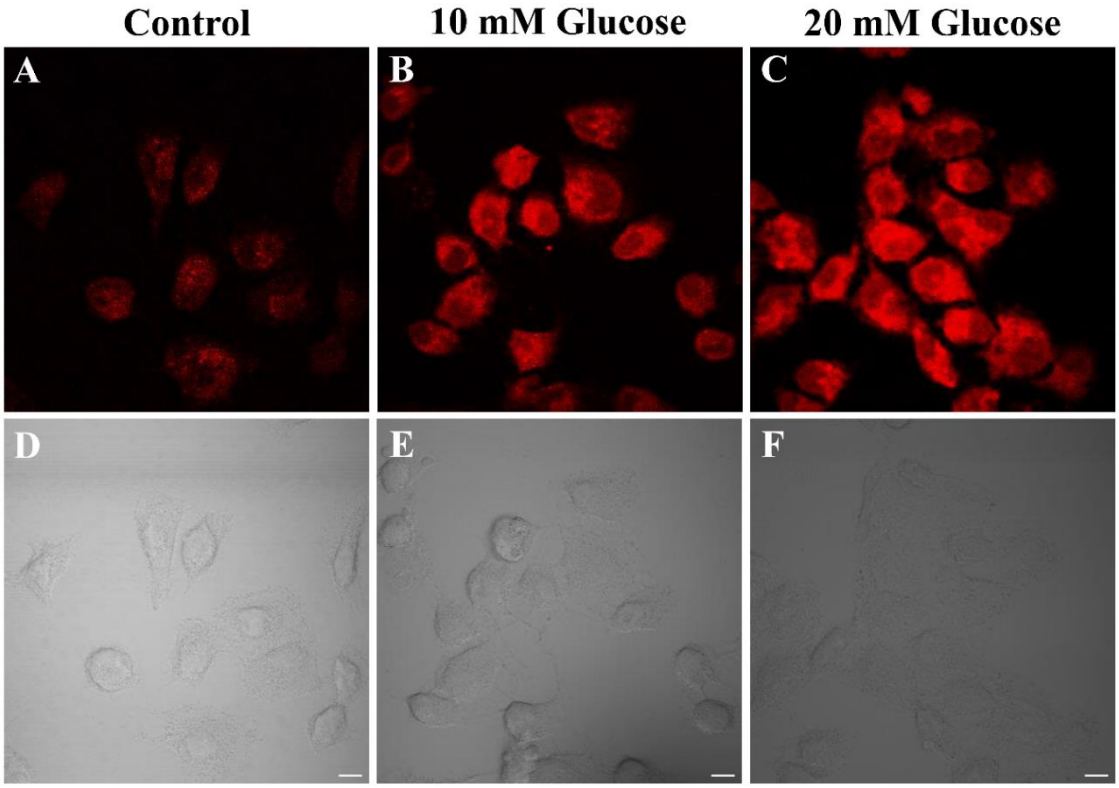

Fig. S15 Fluorescence (A–C) and bright-field (D–F) images of A549 cells pretreated with different concentrations of glucose (10 mM and 20 mM), followed by staining with **Ir2** (10 μM). (A, D) Cells stained with **Ir2** alone (control); (B, E) cells pretreated with 10 mM glucose; (C, F) cells pretreated with 20 mM glucose. Scale bar = 10 μm.

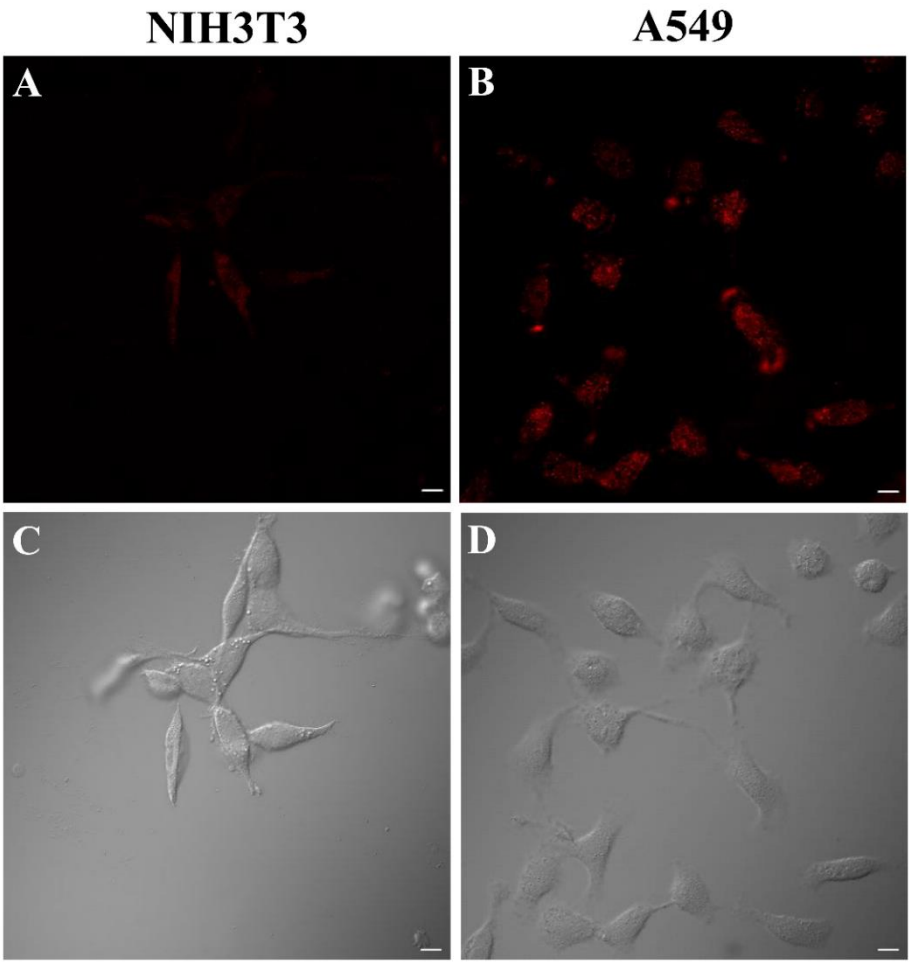

Fig. S16 NAD(P)H imaging in non-cancer (NIH/3T3) and cancer (A549) cells using probe **Ir2**. Fluorescence and) bright-field images of NIH/3T3 cells (A, C) and A549 cells (B, D) incubated with **Ir2** (10 μM). Scale bar = 10 μm.

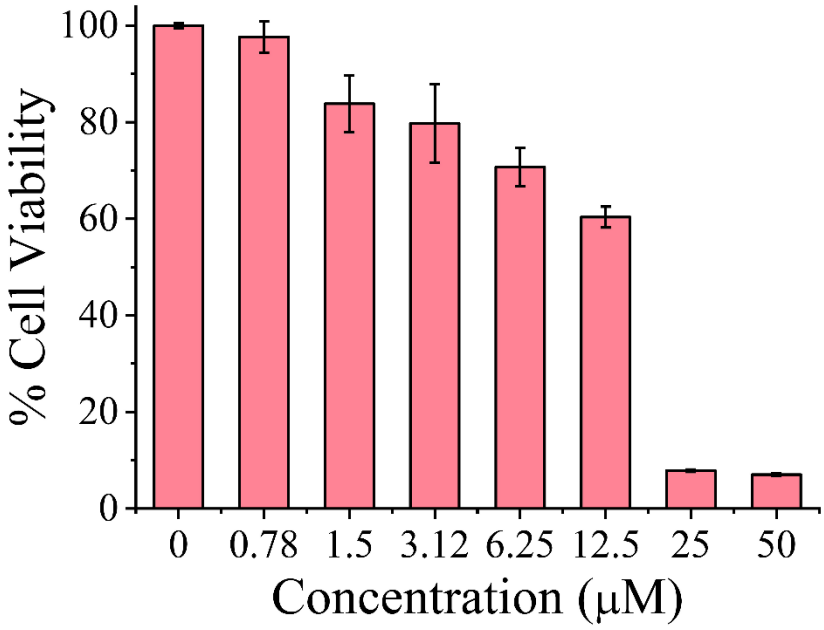

Fig. S17 Cell viability of MCF-7 cells assessed by the MTT assay after 24 h of incubation with varying concentrations of **Ir2**.

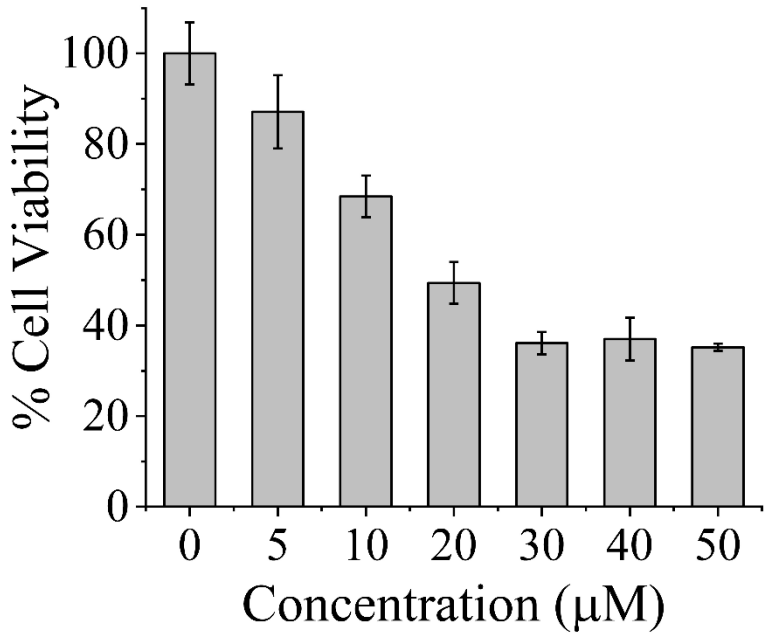

Fig. S18 Cell viability of A549 cells assessed by the MTT assay after 24 h of incubation with varying concentrations of **Ir2**.

Supplementary References

1. A. Gupta, P. Prasad, S. Gupta and P. K. Sasmal, *ACS Appl. Mater. Interfaces*, 2020, **12**, 35967–35976.
2. A. Gautam, A. Gupta, P. Prasad and P. K. Sasmal, *Dalton Trans.*, 2023, **52**, 7843–7853.
3. A. Gupta, A. Gautam, S. Patra, A. Kunwar and P. K. Sasmal, *Chem. Commun.*, 2025, **61**, 7305–7308.
4. L. Wang, J. Zhang, B. Kim, J. Peng, S. N. Berry, Y. Ni, D. Su, J. Lee, L. Yuan and Y. T. Chang, *J. Am. Chem. Soc.*, 2016, **138**, 10394–10397.
5. M. A. Fomin, R. I. Dmitriev, J. Jenkins, D. B. Papkovsky, D. Heindl and B. König, *ACS Sens.*, 2016, **1**, 702–709.
6. A. Podder, S. Koo, J. Lee, S. Mun, S. Khatun, H.-G. Kang, S. Bhuniya and J. S. Kim, *Chem. Commun*., 2019, **55**, 537–540.
7. X. Pan, Y. Zhao, T. Cheng, A. Zheng, A. Ge, L. Zang, K. Xu and B. Tang, *Chem. Sci*., 2019, **10**, 8179–8186.
8. A. Podder, V. P. Murali, S. Deepika, A. Dhamija, S. Biswas, K. K. Maiti and S. Bhuniya, *Anal. Chem.*, 2020, **92**, 12356–12362.
9. D.-C. Duan, J. Liu, Y.-L. Zheng, H. Chen, X. Zhang, Y. Zhang, F. Dai, S. Zhang and B. Zhou, *Anal. Chem.*, 2023, **95**, 1335–1342.
10. Y. Sun, Y. Mao, T. Bai, T. Ye, Y. Lin, F. Wang, L. Li, L. Guo, H. Liu and J. Wang, *Chem. Commun.*, 2024, **60**, 5932–5935.
11. K. Magesh, L. Y. Hsun, S. P. Wu and S. Velmathi, *ACS Appl. Bio Mater.*, 2024, **7**, 5679−5688.
12. D. L. Arachchige, S. K. Dwivedi, S. Jaeger, A. M. Olowolagba, M. Mahmoud, D. R. Tucker, D. R. Fritz, T. Werner, M. Tanasova, R. L. Luck and H. Liu, *ACS Appl. Bio Mater*., 2023, **6**, 3199−3212.
13. L. Jiang, X. Lei, K. Wang, Z. Zhang, F. Wang, S. Lu and X. Chen, *Dyes Pigm.*, 2020, **183**, 108740.
14. J. H. Joo, D. Youn, S. Y. Park, D. S. Shin and M. H. Lee, *Dyes Pigm.*, 2019, **170**, 107561.
15. C. Tu, R. Nagao and A. Y. Louie, *Angew. Chem., Int. Ed.*, 2009, **48**, 6547–6551.
16. S. O. Jung, J. Y. Ahn, S. Kim, S. Yi, M. H. Kim, H. H. Jang, S. H. Seo, M. S. Eomb, S. K. Kim, D. H. Ryu, S. K. Chang, and M. S. Han, *Tetrahedron Lett.*, 2010, **51**, 3775–3778.
17. H. Komatsu, Y. Shindo, K. Oka, J. P. Hill and K. Ariga, *Angew. Chem., Int. Ed.*, 2014, **53**, 3993–3995.
18. R. Zadmard, P. A. Moghaddam, S. Darvishi and M. M. Aghayan, *Tetrahedron*, 2017, **73**, 604–607.
19. Y. Zhao, K. Wei, F. Kong, X. Gao, K. Xu and B. Tang, *Anal. Chem.*, 2019, **91**, 1368–1374.
20. H. Chang, X. Hu, X. Tang, S. Tian, Y. Li, X. Lv and L. Shang, *ACS Sens.*, 2023, **8**, 829−838.
21. H. Wei, Y. Yu, G. Wu, Y. Wang, S. Duan, J. Han, W. Cheng, C. Li, X. Tian and X. Zhang, *Sens. Actuators, B Chem*, 2022, **350**, 130862.

22. M. Li, C. Liu, W. Zhang, L. Xu, M. Yang, Z. Chen, X. Wang, L. Pu, W. Liu and X. Zeng, *J. Mater. Chem., B*, 2021, **9**, 9547.
23. Y. Tian, W.-L. Jiang, W.-X. Wang, G.-J. Mao, Y. Li and C.-Y. Li, *Biomater.*, 2021, **271**, 120736.
24. J. H. Joo, M. Won, S. Y. Park, K. Park, D.-S. Shin, J. S. Kim and M. H. Lee, *Sens. Actuators, B Chem*, 2020, **320**, 128360.
25. M. Maiti, V. P. Murali, D. Selvakumar, A. Podder, K. K. Maiti and S. Bhuniya, *Sens. Actuators B Chem.*, 2019, **299**, 126964.
26. M. Santra, S. Sarkar, Y. W. Jun, Y. J. Reo and K. H. Ahn, *Tetrahedron Lett.*, 2018, **59**, 3210–3213.
27. A. Podder, N. Thirumalaivasan, Y. K. Chao, P. Kukutla, S. P. Wu and S. Bhuniya, *Sens. Actuators, B*, 2020, **324**, 128637.
28. Q. Wang, Y. Z. Zhu, D. B. Chen, J. L. Ou, M. Chen, Y. Feng, W. B. Wang and X. M. Meng, *Talanta*, 2023, **257**, 124393.
29. H. Ito, T. Terai, K. Hanaoka, T. Ueno, T. Komatsu, T. Nagano and Y. Urano, *Chem. Commun.*, 2015, **51**, 8319−8322.
30. S. Shamjith, M. M. Joseph, V. P. Murali, G. S. Remya, J. B. Nair, C. H. Suresh and K. K. Maiti, *Biosens. Bioelectron.*, 2022, **204**, 114087.